Biosensors and Bioelectronics 172 (2021) 112770

Contents lists available at ScienceDirect

Biosensors and Bioelectronics

journal homepage: http://www.elsevier.com/locate/bios

Fully printed prothrombin time sensor for point-of-care testing

Nicholas X. Williams [a], Brittani Carroll [a], Steven G. Noyce [a], Hansel Alex Hobbie [a], Daniel Y. Joh [b], Joseph G. Rogers [c], Aaron D. Franklin [a,d,*]

[a] Department of Electrical and Computer Engineering, Duke University, Durham, NC, 27708, USA
[b] Department of Biomedical Engineering, Duke University, Durham, NC, 27708, USA
[c] Department of Medicine, Duke Clinical Research Institute, Duke University, Durham, NC, 27708, USA
[d] Department of Chemistry, Duke University, Durham, NC, 27708, USA

ARTICLE INFO

Keywords:
Prothrombin time
PT/INR
Coagulation
Printed electronics
Point-of-care
POCT
Impedance

ABSTRACT

With an increasing number of patients relying on blood thinners to treat medical conditions, there is a rising need for rapid, low-cost, portable testing of blood coagulation time or prothrombin time (PT). Current methods for measuring PT require regular visits to outpatient clinics, which is cumbersome and time-consuming, decreasing patient quality of life. In this work, we developed a handheld point-of-care test (POCT) to measure PT using electrical transduction. Low-cost PT sensors were fully printed using an aerosol jet printer and conductive inks of Ag nanoparticles, Ag nanowires, and carbon nanotubes. Using benchtop control electronics to test this impedance-based biosensor, it was found that the capacitive nature of blood obscures the clotting response at frequencies below 10 kHz, leading to an optimized operating frequency of 15 kHz. When printed on polyimide, the PT sensor exhibited no variation in the measured clotting time, even when flexed to a 35 mm bend radius. In addition, consistent PT measurements for both chicken and human blood illustrate the versatility of these printed biosensors under disparate operating conditions, where chicken blood clots within 30 min and anticoagulated human blood clots within 20–100 s. Finally, a low-cost, handheld POCT was developed to measure PT for human blood, yielding 70% lower noise compared to measurement with a commercial potentiostat. This POCT with printed PT sensors has the potential to dramatically improve the quality of life for patients on blood thinners and, in the long term, could be incorporated into a fully flexible and wearable sensing platform.

1. Introduction

Heart failure is a major public health problem affecting over 6.4 million individuals in the United States alone, with over 550,000 new cases emerging annually (Benjamin et al., 2018). Despite therapeutic advances, the disease frequently becomes refractory to medications and eventually requires long-term mechanical circulatory support with ventricular assist devices (VADs), either as a bridge to transplant or destination therapy (Braunwald, 2015; Delgado et al., 2009). Nearly two decades of clinical experience have shown that VAD support leads to significant improvements in survival, functional status, and quality of life (Kirklin et al., 2015). Despite these successes, the persistence of complications currently limits long-term outcomes (Kilic et al., 2015). In particular, the thrombogenic nature of VAD therapy requires long-term anticoagulation treatment, most commonly with the blood thinner warfarin (Morgan et al., 2012). While this reduces the risk of complications that may arise from activation of the coagulation cascade (the most feared being pump thrombosis), chronic anticoagulation inevitably risks bleeding events, which are the most common complication associated with VADs. Several factors can contribute to a change in PT/INR including activity levels, health issues, and medications (Milligan et al., 2002). Periodic blood-based testing is therefore required to measure patients' prothrombin time/international normalized ratio (PT/INR) values to ensure that warfarin levels are within the therapeutic window, which reflect the clotting tendency of blood and hence the extent of anticoagulation. Thus, a monitoring system to ensure adequate coagulation time is a medically dire requirement.

Evidence suggests that earlier identification of potential complications leads to better outcomes, which is the basis for frequent and scheduled monitoring of PT/INR (Birati and Rame, 2015; Blitz, 2014; Kilic et al., 2015; Starling et al., 2013; Stulak et al., 2015). Monitoring typically occurs once every 1–4 weeks, requiring clinic visits in the outpatient setting to obtain blood via venipuncture for testing in centralized laboratories (Bazaev et al., 2015), which is burdensome and

* Corresponding author. Department of Electrical and Computer Engineering, Duke University, Durham, NC, 27708, USA.
E-mail address: aaron.franklin@duke.edu (A.D. Franklin).

https://doi.org/10.1016/j.bios.2020.112770
Received 1 October 2020; Accepted 25 October 2020
Available online 26 October 2020

costly to the patient. Yet, due to warfarin's narrow therapeutic window and the unique hematological changes induced by VADs over time, from a management perspective it is possible that patients may benefit from more frequent testing intervals (Blitz, 2014; Görlinger et al., 2012; Starling et al., 2013; Stulak et al., 2015). Recent studies indicate that patient self-testing of PT/INR at home using point-of-care tests (POCTs) can improve outcomes for VAD patients (Psotka et al., 2016; Svetlichnaya et al., 2016, 2016, 2016).

While patient self-testing of PT/INR with home devices is not a new concept and likely less cumbersome for both patients and the healthcare system, only a small percentage of VAD patients perform self-testing due to the high cost associated with the devices and reagent cartridges (limiting insurance coverage to once-weekly testing) as well as inconsistences in device performance (Potapov et al., 2006; Wittkowsky et al., 2005; Wurster, 2008). For these reasons, an alternative device that offers portable, low-cost, facile, and accurate surveillance of PT/INR may provide significant benefit in the chronic management of advanced heart failure patients on VAD support.

Numerous techniques have been developed for measuring PT/INR, including optical (Lin et al., 2014; Tripathi et al., 2017), viscometric (Northoff et al., 2009; Yao et al., 2018), and electrical transduction (Lei et al., 2013; Ramaswamy et al., 2013; Ur, 1970, 1971, 1977). While each mechanism has its benefits and drawbacks, the simplicity of both the measurement chip and the platform in an electrically transduced sensor enables the development of a robust, low-cost coagulometer for in-home or POC use. To this end, a potential strategy that lends itself to portability is a very low frequency (VLF) impedance measurement, which was initially proposed by Ur et al. (Ur, 1970). Several recent publications have significantly improved upon this original concept of an impedimetric coagulometer. Examples include incorporating microfluidics to minimize the equipment footprint and adding a reference chamber to more readily and reliably visualize the clotting time. Yet, these methods are resource- and time-intensive due to their reliance on lithography-based microfabrication processes in cleanroom environments, which ultimately increase cost and complexity (Lei et al., 2013; Ramaswamy et al., 2013).

Printing electronics has recently gained substantial traction as a promising route for low-cost electronic device fabrication that circumvents the need for cleanroom processing (Adib et al., 2018; Cinti et al., 2017; Khan et al., 2016; Kumar et al., 2019; Lee, 2018; Scheideler and Subramanian, 2019; Shoaie et al., 2017; Song et al., 2018). In addition, nanomaterials can be a powerful tool for highly performance sensors (Cuniberto et al., 2020). Of the available printing techniques, aerosol jet printing (AJP) has attracted interest due to its ability to print on non-planar surfaces, print high aspect-ratio nanomaterial based inks (allowing for the printing of conductive traces at low printing temperatures), and print inks with a broad range of viscosities (Eckstein, 2016; Goodall et al., 2002; Jordan et al., 1996; Seifert et al., 2015; Williams et al., 2019). In brief, AJP functions by aerosolizing ink in an enclosed cartridge using ultrasonic transduction. Aerosolized ink is then delivered to the printer nozzle and eventually the substrate surface by flowing inert gases. Thus far, AJP has been used successfully to fabricate numerous devices, including basic electronic components such as transistors (Cao et al., 2017; Cardenas et al, 2018, 2019; Jabari and Toyserkani, 2015; Jones et al., 2010), sensors (Andrews et al., 2018; Liu et al., 2012; Parate et al., 2020), and even biological materials (Williams et al., 2020).

Here, a fully printed, handheld, impedimetric coagulometer for PT/INR measurement is demonstrated. In order to create a robust device, the electrodes are aerosol jet printed onto a flexible substrate and tested under strain, yielding consistent clotting times under all tested scenarios (glass substrate, polyimide substrate, polyimide substrate bent to a 35 mm bending radius). The operating frequency was optimized at 15 kHz, providing a consistent clotting time to within 2%. The functionality of the device is demonstrated in whole blood derived from both animal and human subjects, lending credence to the ability of this method to function as a broad testing platform. Finally, a handheld sensor with low-cost electronics was designed and shown to have a measurement accuracy to within a standard deviation of the costly, stationary, computer-based testing system. Taken together, these results lay the groundwork for fully printed impedimetric coagulometers, which addresses the unmet need for a low-cost, robust POC device, potentially improving outcomes for VAD patients (and other populations on chronic warfarin) by early detection of derangements in PT/INR.

2. Methods

2.1. Device fabrication and design

An impedance-based device, consisting of two parallel electrodes connected to conductive pads, was printed onto a glass slide. A schematic representation of the device fabrication method is depicted in Fig. S1. All substrates were first cleaned by ultrasonicating in acetone for 5 min, rinsing with deionized (DI) water, and drying using nitrogen. Then the substrates were ultrasonicated in isopropyl alcohol (IPA) for 5 min, rinsed with DI water, and dried with nitrogen.

Silver nanoparticle (AgNP) traces were printed as the conducting electrodes and contact pads (Fig. 1a). Silver nanoparticle (AgNP) ink was prepared by mixing commercial AgNP solution (Ag40 × , UT Dots Inc., USA) with terpinol in a 9:1 ratio to optimize the viscosity for ease of printing and to achieve small line widths. The ultrasonic atomizer mode of an Optomec AJ300 printer was used for printing. 1 mL of the prepared AgNP ink was added to the AJ printer and printed using a 150 μm nozzle. The platen temperature was held at 60 °C during printing, while a sheath gas flow rate of 25 SCCM, an atomizer gas flow rate of 20 SCCM, and an ultrasonic atomizer current of 350 mA were used to print the conductive traces. A print speed of 8 mm s^{-1} was used for all AgNP printing. An image taken with a scanning electron microscope (SEM) of the printed AgNP electrodes can be seen in Fig. 1b – left. After printing, the AgNP traces were annealed in an oven at 200 °C for 1 h to increase conductivity. A spacing of 150 μm between the two electrodes was selected for ease of printing; a labeled schematic of the device can be seen in Fig. 1c.

In order to avoid electrical current measurement range limitations of the computer-tied measurement system, a resistive bridge was printed using either silver nanowires (AgNWs) or unsorted carbon nanotubes (CNTs) (Fig. 1b - right). These inks were selected because of their relatively high conductivity and ease of fabrication with an AJ printer. Neither the AgNWs nor the unsorted CNTs required any post-processing to achieve high conductivities (Williams et al., 2019). Both inks were found to behave in an identical manner and thus were used interchangeably (Fig. S2). High aspect ratio AgNWs (2–6 μm long and 30–50 nm in diameter) were synthesized using the polyol method as described elsewhere (Stewart et al., 2017). 1 mL of 10 mg mL^{-1} ink was added to the ultrasonic atomizer of an Optomec AJ300 and a 200 μm nozzle was used. The platen temperature was held at 80 °C. During printing, a sheath gas flow rate of 40 SCCM, an atomizer gas flow rate of 40 SCCM, and an ultrasonic atomizer current of 350 mA were used.

P3 single-walled unsorted CNTs (Carbon Solutions Inc, USA) were suspended in water at a concentration of 0.1 mg mL^{-1}1 mL of ink was added to the ultrasonic atomizer of an Optomec AJ300 using a 150 μm nozzle. The platen temperature was held at 50 °C. During printing, a sheath gas flow rate of 25 SCCM, an atomizer gas flow rate of 40 SCCM, and an ultrasonic atomizer current of 350 mA were used.

2.2. PT testing of chicken blood

All reagents were stored in a refrigerator at 4 °C before use and removed directly before measurement to ensure all reagents were at the same temperature during testing, as previous reports indicate that clotting time is affected by blood temperature (Valeri et al., 1995). A PalmSens 3600 analyzer, which has a minimum detection current of 1 mA for impedance measurements, was used as a driver and as a

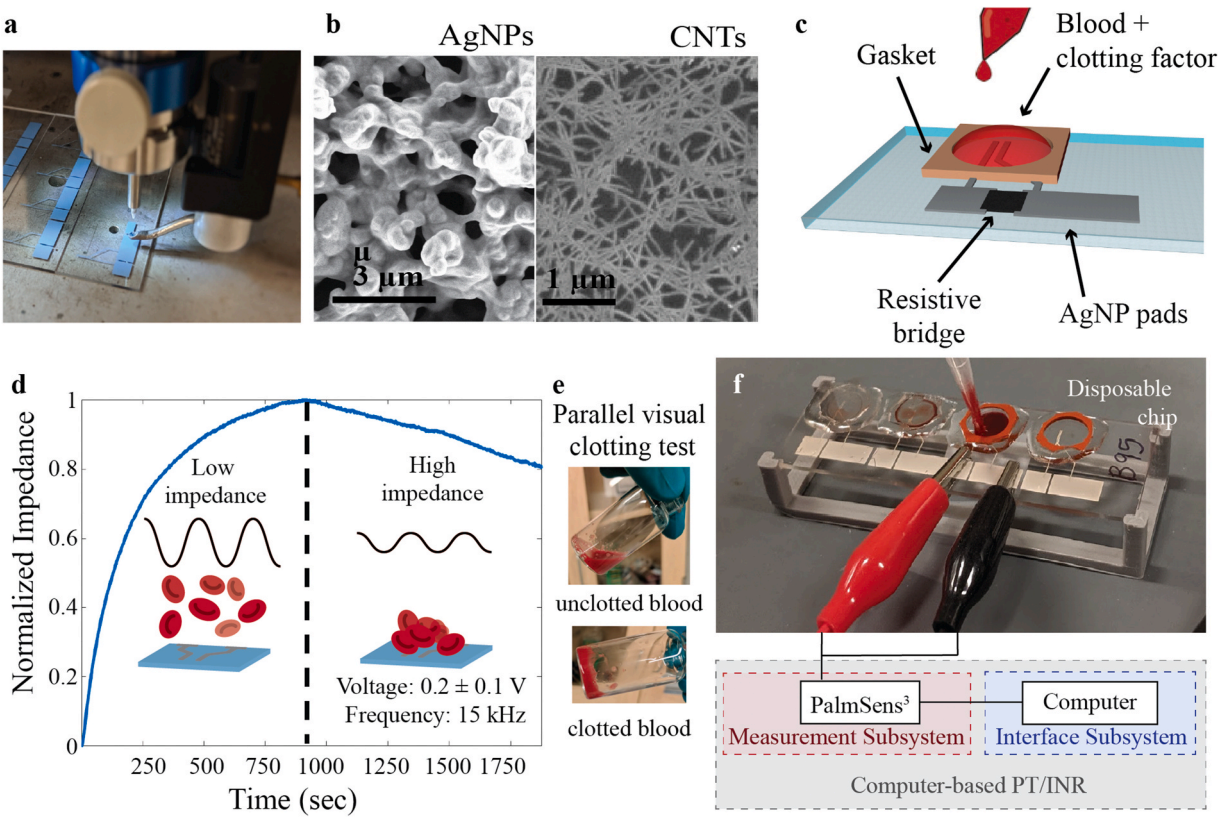

Fig. 1. Printed prothrombin time device fabrication and testing. a) AJ printing of AgNPs for PT/INR device. b) SEM images of (left) AgNP electrode and (right) unsorted carbon nanotube conductive resistive bridge. c) Schematic of device design. d) Representative impedance curve illustrating coagulation test for chicken blood with e) a parallel visual clotting test. The dashed line represents the clotting time as determined by the impedance maximum and the gelatinization of the blood. Before the blood clots, the red blood cells are floating in solution (d – left insert, e – top) and thus the impedance is low; as the blood clots, the red blood cells deposit onto the device and cause the impedance to increase (d – right insert, e – bottom), maximizing at the point of clotting. (f) Picture of testing setup showing blood addition to the sensor and schematic of computer-based impedimetric testing interface. (For interpretation of the references to colour in this figure legend, the reader is referred to the Web version of this article.)

measurement unit. A silicone well was placed around each device to contain all liquid volumes during testing. 250 μL of K2-ethylenediaminetetraacetic acid (EDTA) chelated whole chicken blood (Innovative Research, USA) was added to a vial, along with 500 μL Dade Innovin Derived Fibrinogen (Siemens, USA) human clotting factor, and 3 mM of Ca^{2+} in the form of an aqueous calcium chloride solution. The vial was shaken for 5 s to mix thoroughly and 100 μL of solution was added to the device well. Then 0.2 ± 0.1 V voltage was applied to the device and the impedance response was monitored for 2000 s to observe a clotting response.

2.3. PT testing of human blood

All reagents were stored in a refrigerator at 4 °C before use and removed directly before measurement. A PalmSens 3600 analyzer was used as driver and measurement unit. A silicone well was placed around each device to contain all liquid volumes during testing. Before any liquid was added, voltage was applied to the device. 66 μL of Dade Innovin Derived Fibrinogen (Siemens, USA) human clotting factor and 3 mM Ca^{2+} were added to the well and allowed to settle for 30 s. Afterward, 33 μL of single donor whole human blood (Innovative Research, USA) was added to achieve a total volume of 100 μL in the well. A voltage of 0.2 ± 0.1 V was applied, and the impedance response was continuously monitored for a clotting response for a total of 300 s.

2.4. Calculation of normalized impedance

Due to the varying initial impedances of each device, normalized impedance is calculated and plotted against PT (Fig. S3). Plotting normalized impedance standardizes the data allowing for comparison between tests. Normalized impedance is calculated using the following equation:

$$I_{norm} = \frac{I_t - I_{min}}{I_{max} - I_{min}}$$

where I_{norm} is the normalized impedance, I_t is the measured impedance at a given time point, I_{min} is the minimum impedance in the data set, and I_{max} is the maximum impedance in the data set.

2.5. Handheld device design and testing

A plastic housing case was 3D printed using an Ultimaker 3S 3D printer from Polylactic Acid (PLA). The electronic components consisted of a TFT FeatherWing 2.4" 320 × 240 touchscreen (Adafruit, USA), a Feather M0 Bluefruit LE development board (Adafruit, USA), a PSoC 5LP Development Board (Cypress, USA), and a 3.7 V LiPo battery, along with external resistors and wiring. The majority of the functionality was implemented on the PSoC 5LP chip, utilizing programmable routing between the on-chip analog components. The on-chip digital to analog converter (DAC) was used to output a 0.3 V amplitude sine wave at 15 kHz, centered at 0.5 V. This signal was buffered using an on-chip operational amplifier (op-amp), then passed through a resistor divider before measurement, where one leg of the divider was a 500 Ω resistor and the other was the sensor. The voltage at the far side of the resistor divider was held at 0.5 V by a second on-chip DAC buffered by an on-chip op-amp. The voltage across the sensor was measured by an on-

chip delta-sigma analog to digital converter ($\Delta\sum$ ADC). In addition to analog signal processing, digital filters were implemented alongside firmware that manages the measurement process. These filters consisted of computing an amplitude from each signal cycle observed by the ADC, discarding the first and fourth quartiles, and enacting a running median filter on the remaining values. Many implementation details paralleled those of similar systems described by our group previously (Noyce et al, 2019, 2020).

3. Results and discussion

3.1. 3.1 device characterization

It was first discovered in 1971 that the impedance magnitude of blood increases during coagulation events, with the peak impedance corresponding to the point at which clotting occurs (Ur, 1971). There have been numerous reports on electrical transduction of PT/INR since then, and some results have demonstrated less well-defined signal responses indicating clotting end points than the original impedance curvature (Lei et al., 2013; Zilberman-Rudenko et al., 2018). In this work, the original impedance curvature, with a turning point defining the clotting end point, was replicated and shown to yield a consistent, reproducible response using a fully printed sensor. A representative measurement produced with this printed biosensor can be seen in Fig. 1d, which shows an impedance curve with a distinct impedance maximum corresponding to the clotting time. Before the impedance maximum, the blood has a low viscosity and behaves as a liquid (Fig. 1e (top)); at the maximal impedance, the blood has coagulated to such an extent that it is completely gelatinous (Fig. 1e (bottom)). The impedance change is caused by the sedimentation of red blood cells (RBCs) as the blood shifts from fluidic to gelatinous (Fig. 1d (left insert)); the RBCs have conductivities 30–40 times lower than that of blood plasma (Ur, 1977). As the coagulation pathway progresses, an increasing number of red blood cells deposit onto the electrodes, displacing the conductive plasma and increasing the impedance (Fig. 1d (right insert)). Accordingly, the blood achieves complete coagulation at the moment of maximal impedance as the deposition rate of red blood cells decreases to an insignificant rate. As soon as the blood achieves complete coagulation, clot retraction dominates and the curvature of the graph begins declining again, eventually reaching a nadir at the time of complete clot retraction (Ur, 1971).

It should be noted that the impedance curvature of these devices is the inverse of the original Ur et al. tests, meaning the PT is represented at the maximum impedance instead of the minimum impedance (Ur, 1970). This difference is caused by electrode placement. In the original test, the electrodes were at either end of a glass tube filled with the coagulating blood. As the blood clotted, RBCs deposited at the bottom/walls of the tube, leaving an unperturbed pathway of the highly conductive plasma between each electrode. In contrast, the printed biosensor design herein consists of electrodes deposited onto a flat substrate with the blood placed atop the electrodes. As the blood clots, the RBCs displace the plasma, thus increasing the impedance. While the resulting curve is the inverse of that seen in the original 1971 report, the mechanism remains consistent and the resulting accuracy and reliability remain unchanged or potentially improved based on the smaller and more controlled area being electrically monitored for coagulation.

This impedimetric transduction mechanism makes the electronic method an ideal choice as it is highly sensitive and more reproducible than mechanically based tests due to the lack of moving components (Ur, 1977). Impedance-based measurements have also been shown to yield results that correlate with the standard clinic detection method (optical absorbance), and are more advantageous due to the simplicity and compactness of the measurement apparatus (Blair et al., 1987). Optical techniques often suffer from the inability to measure coagulation with specific clotting factors, which decreases their universal utility (Yang et al., 2013). In addition, the output of impedance measurements can be analyzed by a compact electrical circuit making it an ideal method for the development of a POCT, which would be a major improvement in the measurement of blood coagulation (Berney and Riordan, 2008; Lei et al., 2013).

To realize an electrical POCT, the ability to determine the impedance maximum with precision is key. Moreover, given that a normal PT for humans is less than a minute, a sharp signal and a defined impedance maximum are also required for accurate measurement. Thus, optimization of the device frequency is necessary to develop an impedance-based POCT PT device. To determine the optimal frequency for maximizing impedance response during a clotting event, a frequency sweep was performed from 50 kHz to 1 kHz once every 60 s over the course of a clotting test with chicken blood (Fig. 2a). The 50 kHz maximum was set by a commercial potentiostat testing platform, which has a maximum operating frequency of 50 kHz. As evidenced by the surface plot, the chicken blood clotting time occurred at roughly 1000 s during this test and the impedance response is similar over the majority of the frequency range, indicating that prothrombin time can be accurately measured over a broad frequency range. Cross-sections of the 3D plot provide impedance values over the course of the clotting event at 1 kHz, 10 kHz, 25 kHz, and 50 kHz, shown in Fig. 2b. Ziblerman-Rudenko et al. report high fidelity measurement of clotting time utilizing direct current measurement of blood capacitance (i.e., a response at frequencies below 10 kHz) (Zilberman-Rudenko et al., 2018). We were unable to replicate these results and observed neither a distinct impedance maximum below 10 kHz nor a shift in capacitor time constants, and thus observed no signal response to clotting. Whereas, at frequencies at or above 10 kHz, a distinct impedance maximum can be observed in consistent fashion all the way to 50 kHz.

The 10 kHz minimum frequency limit is attributed to the ionic capacitance of the blood. A circuit diagram representing blood on the impedimetric sensor can be found in Fig. S4a. The impedimetric sensor consists of whole blood impedance in parallel with a conductive bridge resistance, each connected to a contact pad that contains a small amount of resistance. As the whole blood clots, the plasma is displaced from the RBCs, which is what creates the clot capacitance, clot resistance, and plasma resistance in Fig. S4a. At frequencies below 10 kHz, the capacitive response of the blood increases in an inverse power relation (Fig. S4b), which overwhelms the impedance response of the clotting event, nullifying the test. While high frequencies were not investigated in this study, previous reports have explored the impedance of blood at higher frequencies (Abdalla et al., 2010). These results found that blood is dispersive, meaning that its dielectric properties become frequency dependent. At high enough frequencies (MHz range), the dielectric constant of blood decreases precipitously, which would obscure the clotting event due to the relatively low impedance from the settling of red blood cells and plasma displacement (Schwan, 1983). Thus, the ideal operating window for an impedance-based coagulometer is between 10 kHz and 1 MHz. All further testing was performed at 15 kHz.

The repeatability of this fully printed PT biosensor was verified along with the dependence of measured PT on the initial impedance of the sensor. As can be seen in Fig. S5a, the response of the sensors when measured using the commercial potentiostat exhibited a strong correlation between initial impedance magnitude and ability to measure clotting time. At impedance magnitudes that were too high, the majority of the current was transduced through the blood, which does not provide sufficient conductivity to reach an impedance value within the detectability range of the commercial potentiostat. As previously mentioned, AgNWs and CNTs were printed as a resistive bridge to increase the baseline signal to within the range of measurement. Representative images of the impedance behavior of a non-responsive device can be found in Fig. S5b. The resistor increases the background current of the device, thus eliminating the need to measure ultralow currents that are outside of the measurement range of mid-priced sensing platforms, such as the PalmSense^3, which has a minimum limit of detection for impedance spectroscopy of 1 mA.

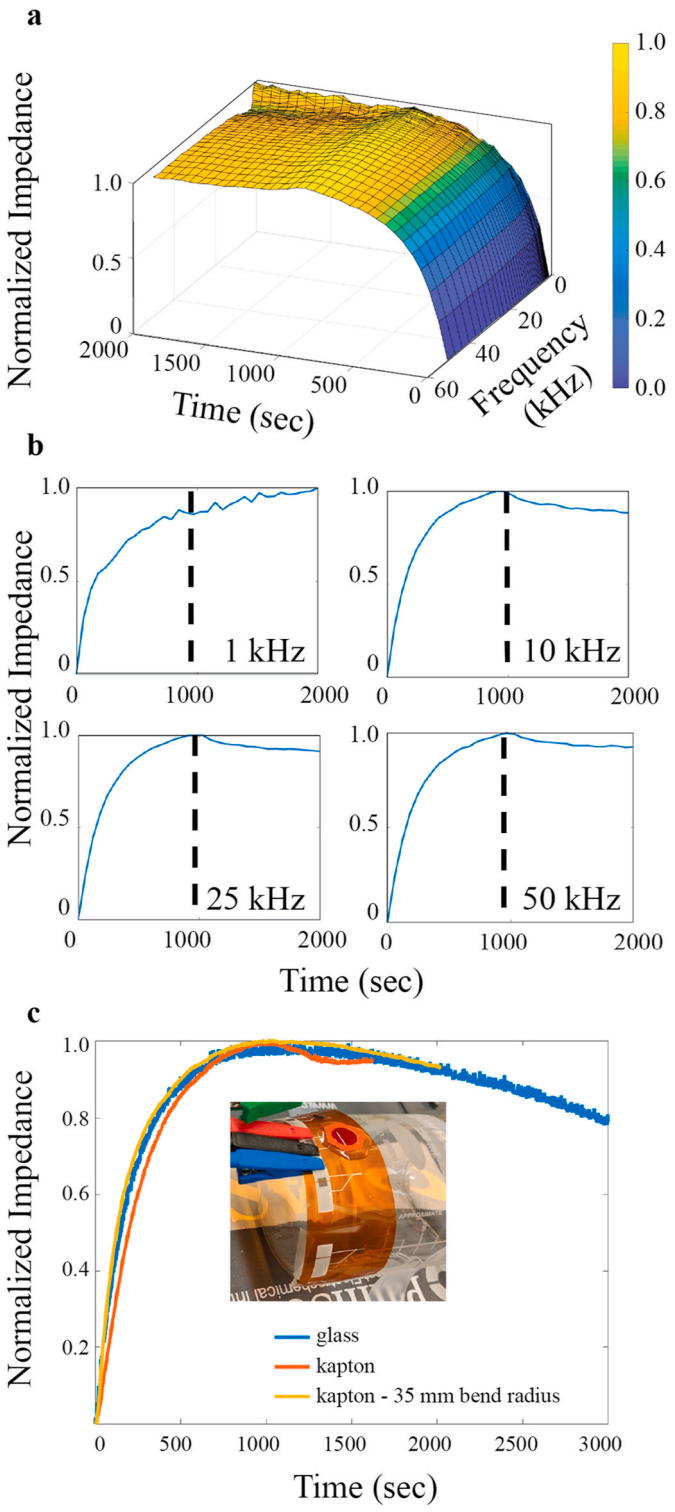

Fig. 2. Impedance-based coagulation testing of chicken blood with printed biosensors. a) Response from sensors tested at frequencies ranging from 1 to 50 kHz over the course of a complete clotting test, revealing the unstable response at sub-10 kHz frequencies. b) Single frequency cross-sections of the full data in a) at 1 kHz (top left), 10 kHz (top right), 25 kHz (bottom left), and 50 kHz (bottom right). c) PT tests at 15 kHz using printed biosensors on various substrates: glass (blue), a Kapton polyimide substrate (orange), and a Kapton polyimide substrate bent at a radius of 35 mm (yellow) with a photo insert of the clotting time test performed while under strain. (For interpretation of the references to colour in this figure legend, the reader is referred to the Web version of this article.)

In printing the resistive bridge, the resistance must be tuned appropriately. While the resistance must be lower than 200 Ω across the gap, it must also be high enough to detect a clotting signal. This testing revealed that at initial impedance values lower than 50 Ω, only a small fraction of the devices functioned. The high background conductivity of the resistive bridge occludes the impedance modulation caused by the coagulation effect. Thus, the device behaves as a blank and no clotting effect can be measured (Fig. S5c).

Multiple tests at various initial impedance values were performed to test the device functionality and repeatability within this determined 50–200 Ω window. Eight representative samples from a larger batch that was selected from multiple different prints were chosen to study the functionality and repeatability of various initial impedances. Fig. S5d shows the impedance spectra from eight tests with various impedance values between 50 and 200 Ω. Fig. S5e shows all eight of the tests overlaid and normalized, demonstrating very similar impedance maximum times. Based on this data, the initial impedance value does not affect the time at which the impedance maximum is observed, and thus does not interfere with the clotting time measurement. Intuitively, this finding is understandable, as the initial impedance value measures the resistive bridge, whereas the impedance maximum measures a magnitude change due to the deposition of RBCs. Furthermore, the consistency of the biosensors with varying initial impedance values also suggests that the morphology difference between printed batches does not make an appreciable impact on the measured PT (Fig. S6). In addition, it can be seen in Fig. S5e that the curvature of the impedance plots both before and after the clot time vary from device to device. We have found that this does not affect the measured clot time but a mechanism for these pre-to-post PT sensor-to-sensor variations is not yet understood.

3.2. *Robust and flexible device testing*

In order to make a truly viable POCT PT/INR test, the single-use measurement chip must be disposable and thus low-cost and robust (Gubala et al., 2012). Fabricating a robust chip decreases the likelihood of damage during both transportation and operation. To fabricate a robust POCT PT/INR device, 125 μm thick Kapton polyimide film is an ideal choice due to its innate flexibility and history as a robust substrate for flexible, printed electronics (Wong and Salleo, 2009). Clotting tests were performed on devices fabricated on a polyimide film and compared to results from a glass slide (Fig. 2c). The results indicated that Kapton-based devices in an unstrained state performed consistently, indicating both that the use of a polyimide film as a robust substrate has no negative impact of the clotting time nor on the ability to measure an impedimetric change and that the measurement of clotting time is substrate agnostic. To further test the flexible device, a clotting test of a printed biosensor on polyimide under a strained state with a 35 mm bend radius was performed (Fig. 2c). This resulted in a consistent clotting time to a device fabricated on a glass slide. Furthermore, the results from the bending test demonstrate that a bent device provides identical performance to an unstrained device, provided that the bend radius is large enough.

While large bending radii do not cause issues with testing, errors may arise at smaller bending radii. Previous reports have explored the impact of bending strain on the electrical resistance of printed conductive traces (Ahn et al., 2009; Valentine et al., 2017; Williams et al., 2019; Zheng et al., 2013). While there is no observable change to the PT/INR when the device is bent to a set radius before the beginning of a test, use cases that involve large modifications to the bending radius during testing could add sufficient impedimetric noise, due to the resistance change in the printed trace, to obscure the clotting result. This is an area that warrants further, more focused study on the impedance-based response noise limits under actively changing strain.

An additional potential for error with bending could be blood pooling away from the device electrodes. If the device is flexed to a small enough bend radius in a tensile state (substrate bent away from the

device), the RBCs may pool at the edges of the well and deposit away from the device electrodes (Fig. S7 (left)). This pooling would obfuscate the clotting result, as the impedimetric response requires deposition of the RBCs directly onto the electrodes. If a large fraction of the blood deposits away from the electrodes, the deposited volume of RBCs over the electrode may not be voluminous enough to accurately measuring the clotting event. On the other hand, if the device was bent in a compressive manner around the device, the blood would most likely pool directly onto the electrodes, which would have no negative effects (Fig. S7 (right)).

Finally, with the addition of a flexible component, this chip has the potential for incorporation into a wearable medical device akin to the wristband smartwatch, which is largely unused real estate. With this incorporation, a PT/INR POCT has the potential for integration into a consumer electronic device, which could have a revolutionary impact on PT testing by allowing for a low-cost and low-effort testing platform that could facilitate testing with almost no decrease in quality of life caused by trips to an outpatient clinic.

3.3. Validation with human blood

While testing the device with chicken blood enabled device development and validation of functionality, the intended use of this device is with whole human blood. Thus, it was imperative to test whether the impedimetric response of the device performed similarly with human blood. The normal clotting time for fresh, whole human blood is on the order of 5–8 min (Lee and White, 1913); however, PT tests are performed by adding a clotting agent to previously anticoagulated blood (Ts'Ao et al., 1979), which has had anticoagulation agents added to it at the time of draw. The coagulation time in a PT test on such anticoagulated blood is on the order of seconds to tens of seconds, which is substantially faster than the 900–1000 s for chicken blood. A representative impedance profile of the clot time for anticoagulated human blood with added Innovin clotting agent (and added calcium to assist with the progression of the clotting pathway) is compared to the clot time of anticoagulated chicken blood with added clotting agent in Fig. 3a.

The error inherent to the procedure developed for chicken blood (mixing the reagents offline, then adding an aliquot of the mixture to the device well) is on the order of 10 s (~1% of the PT for chicken blood), which is similar to the full prothrombin time for anticoagulated human blood. Thus, a new procedure was developed to decrease the measurement error for human blood. The impedance measurement was started without any solution on the device, then 66 μL of Innovin and 0–3 mM calcium were added sequentially to the well and allowed to stabilize for 30 s. Finally, 33 μL blood was added to the well and the impedance was monitored for another 200 s. These volumes were selected to achieve a total addition of 100 μL of liquid to the device. Future research will concentrate on miniaturization of the electrode to decrease the required blood volume down towards the ~3 μl of blood that the average finger prick achieves (Grady et al., 2014). A schematic of this testing procedure can be seen in Fig. 3b. Mixing occurred during the application of the blood due to the small total volume of reactants and the agitation energy from pipetting in the blood. This mixing was enough to give highly repeatable clotting results with a standard deviation of 0.2% for chicken blood (less than 2 s). Only minor changes in PT can be seen in chicken blood with the new procedure as the clotting time is overwhelms the minute change between on-chip and off-chip mixing (Fig. S8).

Given that the clotting time for recombinant tissue factor induced coagulation of K2-EDTA anticoagulated human blood is significantly more rapid than that of chicken blood, further experimentation was required to ensure that the impedance maximum corresponded to the clot time as opposed to an impedance modulation caused by the addition of the blood. Therefore, we found it pertinent to investigate the relationship between an anticoagulant and blood. Given that Dade Innovin volumes were determined by manufacturer recommendation, calcium

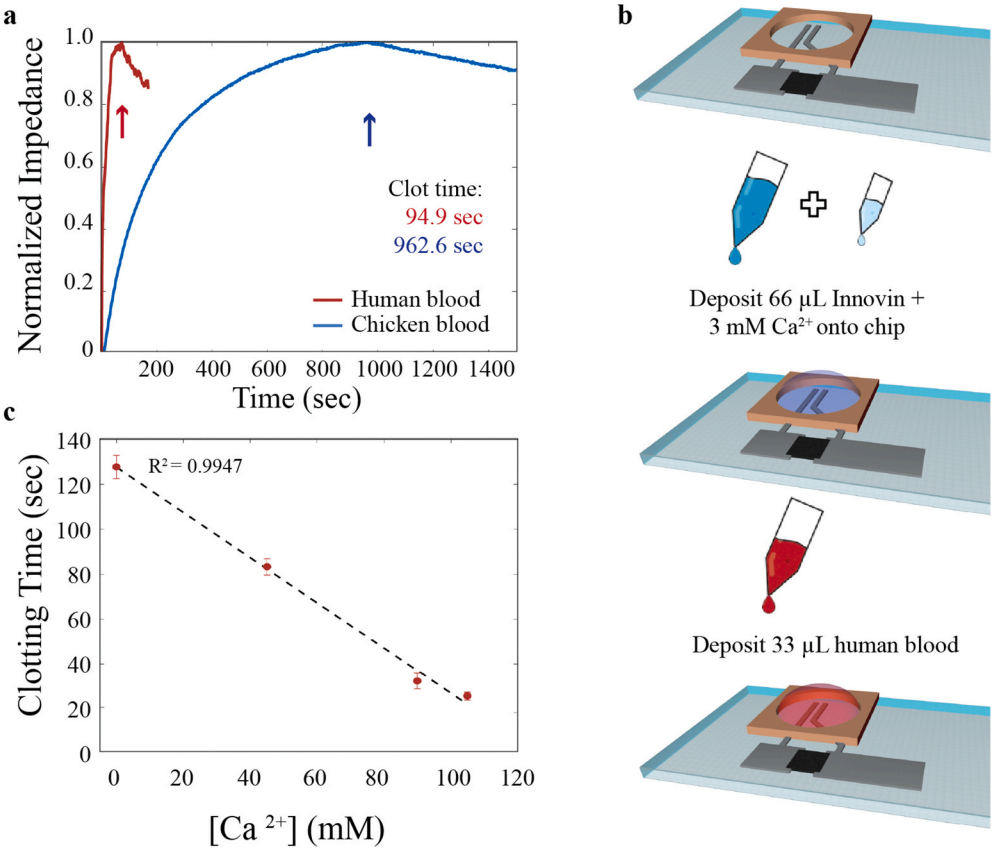

Fig. 3. PT measurements of anticoagulated human blood with printing biosensors. a) Impedance-based PT measurements for human blood (red) and chicken blood (blue). b) Schematics of procedure for testing human blood: fabricate devices and begin impedance test (top), sequentially add Innovin then calcium (middle), wait 30 s for mixing of previous solutions and add human blood (bottom). c) Clotting time for human blood as a function of added calcium concentration. Average ± standard deviation of 4 separate chips is shown with a strong linear correlation fit. (For interpretation of the references to colour in this figure legend, the reader is referred to the Web version of this article.)

concentration was used as a proxy for anticoagulation effect. Four concentrations of calcium were tested (0, 45, 90, and 110 mM) to explore the impact on PT (Fig. 3c). All blood tested was anticoagulated with K2-EDTA, which chelates divalent calcium cations and, through this chelation, prohibits the coagulation pathway from progressing (Marjorie and Borrelli, 1958). The addition of calcium back into the solution overwhelms the chelating ability of the K2-EDTA and thus allows the progression through the coagulation pathway with the addition of Dade Innovin human clotting factor. Previous reports have found a linear correlation between activated partial thromboplastin time and calcium concentration (Strobl et al., 2017), an inverse power relationship between activated clotting time and calcium concentration (Kreuzer et al., 2010; Quick, 2017; Strobl et al., 2017), and a parabolic and decreasing relationship between the PT and calcium (Jaques and Dunlop, 2017). While each of these methods differs in scope, all demonstrate that varying the calcium concentration can alter the kinetics of the clotting reaction. We observed a decreasing, linear relationship between the calcium concentration and the clotting time in the calcium concentrations tested with anticoagulated human blood. While the curvature found was different from that reported in previous studies, the decreasing relationship is similar. The differences may be due to the smaller range observed in this study. The linear trend observed here warrants further, more focused study based on a wider range of calcium concentration and mixing strategies. Regardless of the inconsistencies between this and other studies, the linear relationship indicates that, even at the short clot times associated with PT, this printed biosensor is highly sensitive and accurate, thus demonstrating a universal correlation between calcium concentration and clotting time over multiple detection methods.

From these PT measurements, the INR of a patient can be calculated. Given that different laboratories may have slightly different reagents and procedures, this may lead to variations in recorded PT. Hence, INR is used to ensure that deviations in measured PT are due to a shift in the patient's coagulation time as opposed to differences in operating procedures. INR is determined using the following formula:

$$INR = \left(\frac{PT_{patient}}{PT_{norm}}\right)^{ISI}$$

where PT_{norm} is the average clotting time for a healthy population, $PT_{patient}$ is the measured clotting time, and international sensitivity index (ISI) is a function of the thromboplastin reagent. This equation assumes that all reagents are maintained at a constant 37 °C during testing. There is a strong correlation between PT and reagent temperature which could greatly affect INR and, correspondingly, treatment plans if the patient's blood and the reagents are tested at a non-standard temperature (Lei et al., 2013). In addition, a difficult or traumatic phlebotomy could increase coagulation and provide false readings. (Ranucci and Simioni, 2016) Given these variables, standardization in measurement conditions is a critical concern and could lead to errors if not properly controlled. These are all critical points that warrant more focused study using this fully printed PT sensor.

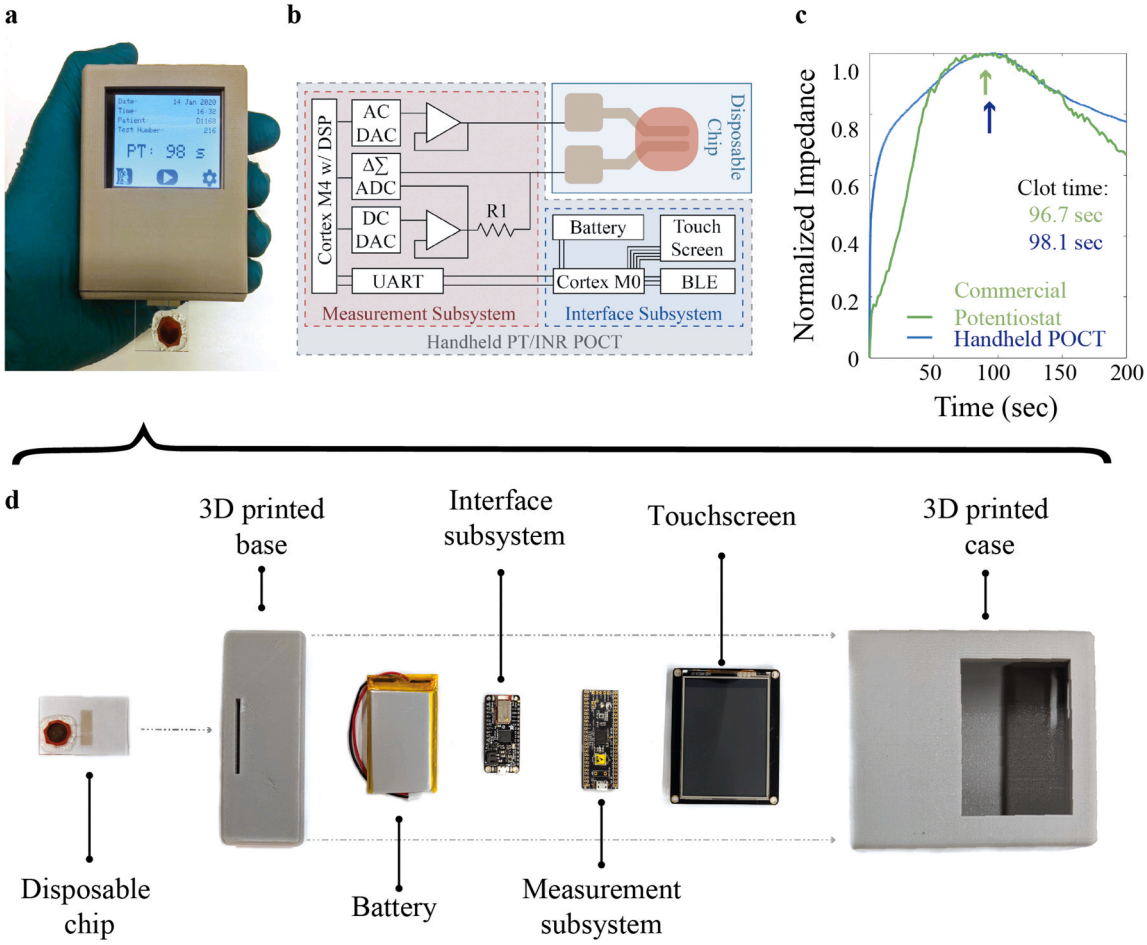

Fig. 4. Handheld POCT system for controlling the printed PT/INR sensor. a) Photo of fully assembled, handheld unit with screen showing results from a PT test. b) Schematic of electronics layout for the handheld measurement system and display. c) PT test comparing a clotting experiment on the commercial potentiostat and the handheld POCT. d) Exploded view of all components in the device with a bill of materials cost of < $50, scalable to < $20.

3.4. Handheld point-of-care test

Finally, given the dire clinical need for a low-cost, POCT for PT/INR, we developed a self-contained, impedance measurement unit in a 3D-printed case to replace the computer-based method (Fig. 4a) for controlling our fully printed PT sensor. Originally, the 5933 CE fully integrated single chip analyzer was considered for use; however, even with the modifications recommended in Berney et al. the sensitivity of the device was too coarse to achieve any modulation with the impedance changes caused by coagulation (Helen Berney and O'Riordan, 2008). Therefore, we designed a new circuit (Fig. 4b) to achieve the required sensitivity with low-cost components (see Methods). All needed measurement and control capabilities were integrated into the system, along with a user-interface display, packaged into a handheld unit.

The handheld device consists of a 3D-printed holder, the measurement and interface boards, a touchscreen, and a battery (Fig. 4d). The circuit makes use of a Cypress PSoC 5LP Dev Board for impedance measurement and digital filtering and is controlled by an Adafruit Feather M0 Bluefruit LE for impedance maximum determination and data communication with a TFT FeatherWing - 2.4″ 320 × 240 Touchscreen for visualization. While there are significant considerations in developing such a system beyond the bill of materials (Wilson et al., 2019), the cost of all parts even at low volume was less than $50. When economies of scale are considered, the component cost for the handheld reader would be below $20. Meanwhile, the printed PT sensor could be transferred to a roll-to-roll printing process compatible with a flexible substrate, making the biosensing component cost sufficiently low for easy accessibility and widespread deployment.

Using this custom handheld unit, the PT for anticoagulated human blood was tested with a printed PT sensor. The result, shown in Fig. 4c, reveals a considerable reduction in the measurement noise with a measured PT that is consistent with that obtained from the computer-based setup. There was less than 2% standard deviation between the tests, which is expected even if the systems were identical, due to differences in blood age, testing temperature, and mixing speed. In addition, with the onboard filtering achievable with the POCT device, the root mean square noise is 70% lower than with the commercial potentiostat, which allows for a more exact determination of the impedance maximum and hence the clotting time. To further ensure accuracy and clinical relevance, future testing will involve the use of clinical samples to provide a comparison between this handheld PT sensor and the clinical standard optical measurement used in hospitals. The ability to test our fully printed PT/INR sensors using such a low-cost, handheld unit opens the way for broad dissemination of such a system to patients. Hence, the fabrication of a handheld POCT system, capable of accurately measuring the PT/INR human blood, as demonstrated herein, has the potential to revolutionize the quality of life for patients with an implanted VAD and moreover any patient that is on warfarin.

4. Conclusion

In conclusion, this work demonstrates the first fully printed biosensor for the low-cost, POC measurement of PT/INR. The testing frequency was optimized at 15 kHz to overcome the high blood capacitance below 10 kHz; no significant improvements in performance were observed at frequencies between 10 and 50 kHz. In addition, a resistive bridge was found to enhance the baseline signal, which enabled significant reduction in the cost of the testing platform, allowing for characterizing the sensors with a simple, low-cost device analyzer. An initial impedance magnitude between 50 and 200 Ω ensured the signal from the clotting event was not masked or too weak for detection. In addition to optimizing the sensor itself, flexible, robust devices fabricated on a polyimide substrate were shown to measure the same clotting time as on a glass slide, even when the polyimide surface was bent to a radius of 35 mm. In addition, we tested the device with both chicken blood and anticoagulated human blood and observed an impedance maximum corresponding to the clotting time of each, despite the disparate times to achieve complete coagulation between the two. Finally, a low-cost, handheld, impedance-based POCT was developed, which could potentially facilitate the at-home PT/INR testing by VAD patients and, more broadly, all patients who need to monitor their PT/INR.

CRediT authorship contribution statement

Nicholas X. Williams: Conceptualization, Methodology, Investigation, Validation, Visualization, Writing - original draft. **Brittani Carroll:** Methodology, Investigation, Validation, Writing - original draft. **Steven G. Noyce:** Investigation, Validation, Writing - original draft. **Hansel Alex Hobbie:** Investigation, Validation, Writing - review & editing. **Daniel Y. Joh:** Conceptualization, Writing - review & editing, Project administration. **Joseph G. Rogers:** Conceptualization, Writing - review & editing, Project administration, Funding acquisition. **Aaron D. Franklin:** Conceptualization, Methodology, Writing - original draft, Supervision, Funding acquisition.

Declaration of competing interest

The authors declare that they have no known competing financial interests or personal relationships that could have appeared to influence the work reported in this paper.

Acknowledgments

This work was supported by the Department of Defense Congressionally Directed Medical Research Program (CDMRP) under award number W81XWH-17-2-0045 and by the National Institutes of Health (NIH) under award numbers 1R21HL141028 and 1R01HL146849.

Appendix A. Supplementary data

Supplementary data related to this article can be found at https://doi.org/10.1016/j.bios.2020.112770.

References

Abdalla, S., Al-ameer, S.S., Al-Magaishi, S.H., 2010. Electrical properties with relaxation through human blood. Biomicrofluidics 4, 1–16. https://doi.org/10.1063/1.3458908.

Adib, M., Eckstein, R., Hernandez-sosa, G., Sommer, M., Lemmer, U., 2018. SnO 2 nanowire-based aerosol jet printed electronic nose as fire detector. IEEE Sensor. J. 18, 494–500.

Ahn, B.Y., Duoss, E.B., Motala, M.J., Guo, X., Park, S.-I., Xiong, Y., Yoon, J., Nuzzo, R.G., Rogers, J.A., Lewis, J.A., 2009. Omnidirectional printing of flexible, stretchable, and spanning silver microelectrodes. Science 323, 1590–1593. https://doi.org/10.1126/science.1168375.

Andrews, J.B., Cardenas, J.A., Lim, C.J., Noyce, S.G., Mullett, J., Franklin, A.D., 2018. Fully printed and flexible carbon nanotube transistors for pressure sensing in automobile tires. IEEE Sensor. J. 18, 7875–7880. https://doi.org/10.1109/JSEN.2018.2842139.

Bazaev, I.A., Przhiyalgovskaya, A.V., Rudenko, P.A., Tronin, A.V., Lifshits, G.I., 2015. Modern methods for measuring parameters of blood coagulation. Biomed. Eng. 49, 136–141. https://doi.org/10.1007/s10527-015-9515-9.

Benjamin, E.J., Virani, S.S., Callaway, C.W., Chamberlain, A.M., Chang, A.R., Cheng, S., Chiuve, S.E., Cushman, M., Delling, F.N., Deo, R., De Ferranti, S.D., Ferguson, J.F., Fornage, M., Gillespie, C., Isasi, C.R., Jiménez, M.C., Jordan, L.C., Judd, S.E., Lackland, D., Lichtman, J.H., Lisabeth, L., Liu, S., Longenecker, C.T., Lutsey, P.L., MacKey, J.S., Matchar, D.B., Matsushita, K., Mussolino, M.E., Nasir, K., O'Flaherty, M., Palaniappan, L.P., Pandey, A., Pandey, D.K., Reeves, M.J., Ritchey, M.D., Rodriguez, C.J., Roth, G.A., Rosamond, W.D., Sampson, U.K.A., Satou, G.M., Shah, S.H., Spartano, N.L., Tirschwell, D.L., Tsao, C.W., Voeks, J.H., Willey, J.Z., Wilkins, J.T., Wu, J.H.Y., Alger, H.M., Wong, S.S., Muntner, P., 2018. Heart disease and stroke statistics - 2018 update: a report from the American heart association. Circulation. https://doi.org/10.1161/CIR.0000000000000558.

Berney, B.H., Riordan, J.J.O., 2008. Impedance measurement monitors blood coagulation. Analog. Dialogue 42, 2–4.

Birati, E.Y., Rame, J.E., 2015. Diagnosis and management of LVAD thrombosis. Curr. Treat. Options Cardiovasc. Med. 17 https://doi.org/10.1007/s11936-014-0361-y.

Blair, S.D., Menashi, S., Samson, D., Greenhalgh, R.M., 1987. Whole blood clotting tests: an evaluation of five methods. Clin. Lab. Haematol. 9, 91–94. https://doi.org/10.1111/j.1365-2257.1987.tb01387.x.

Blitz, A., 2014. Pump thrombosis—a riddle wrapped in a mystery inside an enigma keynote lecture series. Ann. Cardiothorac. Surg. 3, 450–471. https://doi.org/10.3978/j.issn.2225-319X.2014.09.10.

Braunwald, E., 2015. The war against heart failure: the Lancet lecture. Lancet 385, 812–824. https://doi.org/10.1016/S0140-6736(14)61889-4.

Cao, C., Andrews, J.B., Franklin, A.D., 2017. Completely printed, flexible, stable, and hysteresis-free carbon nanotube thin-film transistors via aerosol jet printing. Adv. Electron. Mater. 3, 1–10. https://doi.org/10.1002/aelm.201700057.

Cardenas, J.A., Catenacci, M.J., Andrews, J.B., Williams, N.X., Wiley, B.J., Franklin, A.D., 2018. In-place printing of carbon nanotube transistors at low temperature. ACS Appl. Nano Mater 1, 1863–1869. https://doi.org/10.1021/acsanm.8b00269.

Cardenas, J.A., Upshaw, S., Williams, N.X., Catenacci, M.J., Wiley, B.J., Franklin, A.D., 2019. Impact of morphology on printed contact performance in carbon nanotube thin-film transistors. Adv. Funct. Mater. 29, 1–7. https://doi.org/10.1002/adfm.201805727.

Cinti, S., Mazzaracchio, V., Cacciotti, I., Moscone, D., Arduini, F., 2017. Carbon black-modified electrodes screen-printed onto paper towel, waxed paper and parafilm M®. Sensors 17, 2267. https://doi.org/10.3390/s17102267.

Cuniberto, E., Alharbi, A., Wu, T., Huang, Z., Sardashti, K., You, K.D., Kisslinger, K., Taniguchi, T., Watanabe, K., Kiani, R., Shahrjerdi, D., 2020. Nano-engineering the material structure of preferentially oriented nano-graphitic carbon for making high-performance electrochemical micro-sensors. Sci. Rep. 10, 1–11. https://doi.org/10.1038/s41598-020-66408-9.

Delgado, R.M., Conte, J.V., Rogers, J.G., Tatooles, A.J., Slaughter, M.S., Farrar, D.J., Feldman, D., Long, J.W., Frazier, O.H., Wozniak, T.C., Milano, C.A., Russell, S.D., Ghumman, W., Sun, B., 2009. Advanced heart failure treated with continuous-flow left ventricular assist device. N. Engl. J. Med. 361, 2241–2251. https://doi.org/10.1056/nejmoa0909938.

Eckstein, R., 2016. Aerosol Jet Printed Electronic Devices and Systems.

Goodall, S., Chew, N., Chan, K., Auriac, D., Waters, M.J., 2002. Aerosolization of protein solutions using thermal inkjet technology. J. Aerosol Med. 15, 351–357. https://doi.org/10.1089/089426802760292717.

Görlinger, K., Bergmann, L., Dirkmann, D., 2012. Coagulation management in patients undergoing mechanical circulatory support. Best Pract. Res. Clin. Anaesthesiol. 26, 179–198. https://doi.org/10.1016/j.bpa.2012.04.003.

Grady, M., Pineau, M., Pynes, M.K., Katz, L.B., Ginsberg, B., 2014. A clinical evaluation of routine blood sampling practices in patients with diabetes: impact on fingerstick blood volume and pain. J. Diabetes Sci. Technol. 8, 691–698. https://doi.org/10.1177/1932296814533172.

Gubala, V., Harris, L.F., Ricco, A.J., Tan, M.X., Williams, D.E., 2012. Point of care diagnostics: status and future. Anal. Chem. https://doi.org/10.1021/ac2030199.

Helen Berney, H., O'Riordan, J.J., 2008. Impedance measurement monitors blood coagulation | analog devices. Analog. Dialogue 42, 2–4.

Jabari, E., Toyserkani, E., 2015. Micro-scale aerosol-jet printing of graphene interconnects. Carbon N. Y. 91, 321–329. https://doi.org/10.1016/j.carbon.2015.04.094.

Jaques, L.B., Dunlop, A.P., 2017. The effect of calcium concentration on the prothrombin time of dogs treated with dicumarol. Am. J. Physiol. Content 143, 355–360. https://doi.org/10.1152/ajplegacy.1945.143.3.355.

Jones, C.S., Lu, X., Renn, M., Stroder, M., Shih, W.S., 2010. Aerosol-jet-printed, high-speed, flexible thin-film transistor made using single-walled carbon nanotube solution. Microelectron. Eng. 87, 434–437. https://doi.org/10.1016/j.mee.2009.05.034.

Jordan, J.D., Dunbar, R.A., Bright, F.V., 1996. Aerosol-generated sol-gel-derived thin films as biosensing platforms. Anal. Chim. Acta 332, 83–91. https://doi.org/10.1016/0003-2670(96)00154-7.

Khan, Y., Garg, M., Gui, Q., Schadt, M., Gaikwad, A., Han, D., Yamamoto, N.A.D., Hart, P., Welte, R., Wilson, W., Czarnecki, S., Poliks, M., Jin, Z., Ghose, K., Egitto, F., Turner, J., Arias, A.C., 2016. Flexible hybrid electronics: direct interfacing of soft and hard electronics for wearable health monitoring. Adv. Funct. Mater. 26, 8764–8775. https://doi.org/10.1002/adfm.201603763.

Kilic, A., Acker, M.A., Atluri, P., 2015. Dealing with surgical left ventricular assist device complications. J. Thorac. Dis. 7, 2158–2164. https://doi.org/10.3978/j.issn.2072-1439.2015.10.64.

Kirklin, J.K., Naftel, D.C., Pagani, F.D., Kormos, R.L., Stevenson, L.W., Blume, E.D., Myers, S.L., Miller, M.A., Baldwin, J.T., Young, J.B., 2015. Seventh INTERMACS annual report: 15,000 patients and counting. J. Heart Lung Transplant. 34, 1495–1504. https://doi.org/10.1016/j.healun.2015.10.003.

Kreuzer, M., Ahlenstiel, T., Kanzelmeyer, N., Ehrich, J.H.H., Pape, L., 2010. Management of regional citrate anticoagulation in pediatric high-flux dialysis: activated coagulation time versus post-filter ionized calcium. Pediatr. Nephrol. 25, 1305–1310. https://doi.org/10.1007/s00467-010-1483-4.

Kumar, R., Johnson, K.M., Williams, N.X., Subramanian, V., 2019. Scaling printable Zn-Ag2O batteries for integrated electronics. Adv. Energy Mater. 1803645, 1803645. https://doi.org/10.1002/aenm.201803645.

Lee, R.I., White, P.D., 1913. A clinical study of the coagulation time of blood. Am. J. Med. Sci. 145, 495–503. https://doi.org/10.1097/00000441-191304000-00004.

Lee, Y., 2018. Direct printing of capacitive touch sensors on flexible substrates by additive E-jet printing with silver. Nano 139, 1–7. https://doi.org/10.1115/1.4034663.

Lei, K.F., Chen, K.H., Tsui, P.H., Tsang, N.M., 2013. Real-time electrical impedimetric monitoring of blood coagulation process under temperature and hematocrit variations conducted in a microfluidic chip. PloS One 8. https://doi.org/10.1371/journal.pone.0076243.

Lin, Y.-C., Yen, S.-C., Cheng, S., Huang, T., 2014. Effectiveness of holographic optical element module sensor in measuring blood prothrombin time. Inst. Phys. 1–12.

Liu, R., Ding, H., Lin, J., Shen, F., Cui, Z., Zhang, T., 2012. Fabrication of platinum-decorated single-walled carbon nanotube based hydrogen sensors by aerosol jet printing. Nanotechnology 23. https://doi.org/10.1088/0957-4484/23/50/505301.

Marjorie, B., Borrelli, J., 1958. Some effects of divalent cations on the clotting mechanism and the platelets of EDTA blood. J. Appl. Physiol. 12, 453–460.

Milligan, P.E., Banet, G.A., Waterman, A.D., Gatchel, S.K., Gage, B.F., 2002. Substitution of generic warfarin for Coumadin in an HMO setting. Ann. Pharmacother. 36, 764–768. https://doi.org/10.1345/aph.1A327.

Morgan, J.A., Paone, G., Nemeh, H.W., Henry, S.E., Patel, R., Vavra, J., Williams, C.T., Lanfear, D.E., Tita, C., Brewer, R.J., 2012. Gastrointestinal bleeding with the HeartMate II left ventricular assist device. J. Heart Lung Transplant. 31, 715–718. https://doi.org/10.1016/j.healun.2012.02.015.

Northoff, H., Drechsel, H., Wendel, H.-P., Gehring, F.K., Sinn, S., Müller, L., Ziegler, C., 2009. Investigation of prothrombin time in human whole-blood samples with a quartz crystal biosensor. Anal. Chem. 82, 658–663. https://doi.org/10.1021/ac9021117.

Noyce, S.G., Doherty, J.L., Cheng, Z., Han, H., Bowen, S., Franklin, A.D., 2019. Electronic stability of carbon nanotube transistors under long-term bias stress. Nano Lett. 19, 1460–1466. https://doi.org/10.1021/acs.nanolett.8b03986.

Noyce, S.G., Doherty, J.L., Zauscher, S., Franklin, A.D., 2020. Understanding and mapping sensitivity in MoS2 field-effect-transistor-based sensors. ACS Nano 14, 11637–11647. https://doi.org/10.1021/acsnano.0c04192.

Parate, K., Pola, C.C., Rangnekar, S.V., Mendivelso-Perez, D.L., Smith, E.A., Hersam, M.C., Gomes, C.L., Claussen, J.C., 2020. Aerosol-jet-printed graphene electrochemical histamine sensors for food safety monitoring. 2D Mater. 7, 034002 https://doi.org/10.1088/2053-1583/ab8919.

Potapov, E.V., Jurmann, M.J., Drews, T., Pasic, M., Loebe, M., Weng, Y., Hetzer, R., 2006. Patients supported for over 4 years with left ventricular assist devices. Eur. J. Heart Fail. 8, 756–759. https://doi.org/10.1016/j.ejheart.2006.02.003.

Psotka, M.A., Svetlichnaya, J., Kassemos, M., Kobasic, K., McClure, K., Sharma, S., Nam, Y., Selby, V.N., Janmohamed, M., Marco, T. De, Wieselthaler, G., Klein, L., 2016. Abstract 17522: home monitoring is associated with fewer hospital readmissions following left ventricular assist device implantation. Circulation 134, A17522. https://doi.org/10.1161/circ.134.suppl_1.17522. A17522.

Quick, A.J., 2017. Calcium in the coagulation of the blood. Am. J. Physiol. Content 131, 455–464. https://doi.org/10.1152/ajplegacy.1940.131.2.455.

Ramaswamy, B., Yeh, Y.-T.T., Zheng, S.-Y., 2013. Microfluidic device and system for point-of-care blood coagulation measurement based on electrical impedance sensing. Sensor. Actuator. B Chem. 180, 21–27. https://doi.org/10.1016/j.snb.2011.11.031.

Ranucci, M., Simioni, P., 2016. Point-of-Care Tests for Severe Hemorrhage, Point-of-Care Tests for Severe Hemorrhage. https://doi.org/10.1007/978-3-319-24795-3.

Scheideler, W., Subramanian, V., 2019. Printed flexible and transparent electronics: enhancing low-temperature processed metal oxides with 0D and 1D nanomaterials. Nanotechnology 30. https://doi.org/10.1088/1361-6528/ab1167.

Schwan, H.P., 1983. Electrical properties of blood and its constituents: alternating current spectroscopy. Blut 46, 185–197. https://doi.org/10.1007/BF00320638.

Seifert, T., Sowade, E., Roscher, F., Wiemer, M., Gessner, T., Baumann, R.R., 2015. Additive manufacturing technologies compared: morphology of deposits of silver ink using inkjet and aerosol jet printing. Ind. Eng. Chem. Res. 54, 769–779. https://doi.org/10.1021/ie503636c.

Shoaie, N., Forouzandeh, M., Omidfar, K., 2017. Highly sensitive electrochemical biosensor based on polyaniline and gold nanoparticles for DNA detection. IEEE Sensor. J. 18, 1835–1843. https://doi.org/10.1109/JSEN.2017.2787024.

Song, D., Zare Bidoky, F., Hyun, W.J., Walker, S.B., Lewis, J.A., Frisbie, C.D., 2018. All-printed, self-aligned carbon nanotube thin-film transistors on imprinted plastic substrates. ACS Appl. Mater. Interfaces 10, 15926–15932. https://doi.org/10.1021/acsami.8b01581.

Starling, R.C., Moazami, N., Silvestry, S.C., Ewald, G., Rogers, J.G., Milano, C.A., Rame, J.E., Acker, M.A., Blackstone, E.H., Ehrlinger, J., Thuita, L., Mountis, M.M., Soltesz, E.G., Lytle, B.W., Smedira, N.G., 2013. Unexpected abrupt increase in left ventricular assist device thrombosis. N. Engl. J. Med. 370, 33–40. https://doi.org/10.1056/nejmoa1313385.

Stewart, I.E., Kim, M.J., Wiley, B.J., 2017. Effect of morphology on the electrical resistivity of silver nanostructure films. ACS Appl. Mater. Interfaces 9, 1870–1876. https://doi.org/10.1021/acsami.6b12289.

Strobl, K., Harm, S., Weber, V., Hartmann, J., 2017. The role of ionized calcium and magnesium in regional citrate anticoagulation and its impact on inflammatory parameters. Int. J. Artif. Organs 40, 15–21. https://doi.org/10.5301/ijao.5000558.

Stulak, J.M., Sharma, S., Maltais, S., 2015. Management of pump thrombosis in patients with left ventricular assist devices. Am. J. Cardiovasc. Drugs 15, 89–94. https://doi.org/10.1007/s40256-014-0102-3.

Svetlichnaya, J., Psotka, MiA., Kassemos, M., Kobasic, K., McClure, K., Sharma, S., Nam, Y., Selby, V.N., Janmohamed, M., Marco, T. De, Wieselthaler, G.M., Klein, L., 2016. Abstract 19132: home monitoring is associated with fewer gastrointestinal bleeding events following left ventricular assist device implantation. Circulation 134, A19132. https://doi.org/10.1161/circ.134.suppl_1.19132.

Tripathi, M.M., Egawa, S., Wirth, A.G., Tshikudi, D.M., Van Cott, E.M., Nadkarni, S.K., 2017. Clinical evaluation of whole blood prothrombin time (PT) and international normalized ratio (INR) using a Laser Speckle Rheology sensor. Sci. Rep. 7, 9169. https://doi.org/10.1038/s41598-017-08693-5.

Ts'Ao, C., Galluzzo, T.S., Lo, R., Peterson, K.G., 1979. Whole-blood clotting time, activated partial thromboplastin time, and whole-blood recalcification time as heparin monitoring tests. Am. J. Clin. Pathol. 71, 17–21. https://doi.org/10.1093/ajcp/71.1.17.

Ur, A., 1977. Analysis and interpretation of the impedance blood coagulation curve. Am. J. Clin. Pathol. 67, 470–476.

Ur, A., 1971. Detection of clot retraction through changes of the electrical impedance of blood during coagulation. Am. J. Clin. Pathol. 56, 713–718.
Ur, A., 1970. Changes in the electrical impedance of blood during coagulation. Nat. Publ. Gr. 226, 269–270.
Valentine, A.D., Busbee, T.A., Boley, J.W., Raney, J.R., Chortos, A., Kotikian, A., Berrigan, J.D., Durstock, M.F., Lewis, J.A., 2017. Hybrid 3D printing of soft electronics. Adv. Mater. 29, 1–8. https://doi.org/10.1002/adma.201703817.
Valeri, C.r., MacGregor, H., Cassidy, G., Tinney, R., Pompeii, F., 1995. The effects of temperature on bleeding time and clotting time in normal volunteers. Crit. Care Med. 23, 698–704.
Williams, N.X., Noyce, S., Cardenas, J.A., Catenacci, M., Wiley, B.J., Franklin, A.D., 2019. Silver nanowire inks for direct-write electronic tattoo applications. Nanoscale 11, 14294–14302. https://doi.org/10.1039/c9nr03378e.
Williams, N.X., Watson, N., Joh, D.Y., Chilkoti, A., Franklin, A.D., 2020. Aerosol jet printing of biological inks by ultrasonic delivery. Biofabrication 12, 025004. https://doi.org/10.1016/j.procbio.2006.09.007.
Wilson, D.J., Kumar, A.A., Mace, C.R., 2019. Overreliance on cost reduction as a featured element of sensor design. ACS Sens. 4, 1120–1125. https://doi.org/10.1021/acssensors.9b00260.
Wittkowsky, A.K., Sekreta, C.M., Nutescu, E.A., Ansell, J., 2005. Barriers to patient self-testing of prothrombin time: National survey of anticoagulation practitioners. Pharmacotherapy 25, 265–269. https://doi.org/10.1592/phco.25.2.265.56949.
Wong, W.S., Salleo, A., 2009. Flexible Electronics: Materials and Applications, Electronic Materials: Science & Technology. Springer US.
Wurster, M.W., 2008. Patient self-testing for management of anticoagulation therapy: Challenges. J. Thromb. Thrombolysis 25, 16–17. https://doi.org/10.1007/s11239-007-0097-6.
Yang, C.L., Huang, S.J., Chou, C.W., Chiou, Y.C., Lin, K.P., Tsai, M.S., Young, K.C., 2013. Design and evaluation of a portable optical-based biosensor for testing whole blood prothrombin time. Talanta 116, 704–711. https://doi.org/10.1016/j.talanta.2013.07.064.
Yao, J., Feng, B., Zhang, Z., Li, C., Zhang, W., Guo, Z., Zhao, H., Zhou, L., 2018. Blood coagulation testing smartphone platform using quartz crystal microbalance dissipation method. Sensors 18. https://doi.org/10.3390/s18093073.
Zheng, Y., He, Z., Gao, Y., Liu, J., 2013. Direct desktop printed-circuits-on-paper flexible electronics. Sci. Rep. 3, 1–7. https://doi.org/10.1038/srep01786.
Zilberman-Rudenko, J., White, R.M., Zilberman, D.A., Lakshmanan, H.H.S., Rigg, R.A., Shatzel, J.J., Maddala, J., McCarty, O.J.T., 2018. Design and utility of a point-of-care microfluidic platform to assess hematocrit and blood coagulation. Cell. Mol. Bioeng. 11, 519–529. https://doi.org/10.1007/s12195-018-0541-z.